Published in final edited form as:
Ann Biomed Eng. 2014 April ; 42(4): 858–870. doi:10.1007/s10439-013-0949-5.

A biophysically-based finite state machine model for analysing gastric experimental entrainment and pacing recordings

Shameer Sathar, **Mark L. Trew**, **Peng Du**, **Greg O' Grady**, and **Leo K. Cheng**
Auckland Bioengineering Institute, The University of Auckland, New Zealand.

Abstract

Gastrointestinal motility is coordinated by slow waves (SWs) generated by the interstitial cells of Cajal (ICC). Experimental studies have shown that SWs spontaneously activate at different intrinsic frequencies in isolated tissue, whereas in intact tissues they are entrained to a single frequency. Gastric pacing has been used in an attempt to improve motility in disorders such as gastroparesis by modulating entrainment, but the optimal methods of pacing are currently unknown. Computational models can aid in the interpretation of complex *in-vivo* recordings and help to determine optical pacing strategies. However, previous computational models of SW entrainment are limited to the intrinsic pacing frequency as the primary determinant of the conduction velocity, and are not able to accurately represent the effects of external stimuli and electrical anisotropies. In this paper, we present a novel computationally efficient method for modelling SW propagation through the ICC network while accounting for conductivity parameters and fiber orientations. The method successfully reproduced experimental recordings of entrainment following gastric transection and the effects of gastric pacing on SW activity. It provides a reliable new tool for investigating gastric electrophysiology in normal and diseased states, and to guide and focus future experimental studies.

Keywords

gastric electrophysiology; finite-state machine; entrainment; gastric pacing; interstitial cells of Cajal

1. Introduction

Slow wave (SW) activity underpins phasic contractions in much of the gastrointestinal tract (GI) tract. SWs are generated and actively propagated by networks of interstitial cells of Cajal (ICC), which in turn activate the adjacent smooth muscle cells.[27] Isolated ICC excite at unique intrinsic frequencies with a declining gradient along the aboral direction of the stomach.[12,14] However, in the intact tissue, ICC are entrained to the single highest frequency in their syncytium, which is a key factor in coordinated motility in the GI tract.[27] Recent studies have shown that degradation of ICC are associated with GI motility disorders such as gastroparesis and slow transit constipation.[13,27]

Gastric pacing can extrinsically entrain and control ICC frequencies, and has been applied in an attempt to improve motility and symptoms associated with gastroparesis and other motility disorders.[19,20] However, determining the most efficient pacing parameters such as

Correspondence Dr. Leo K. Cheng Private Bag 92019, Auckland 1142, New Zealand. l.cheng@auckland.ac.nz Telephone: +64 9 373 7599 Facsimile: +64 9 367 7157.

stimulus location, amplitude, width and frequency currently typically depends on extensive trial-and-error experiments in animal models; this is inefficient and costly.[4]

Mathematical models offer a virtual medium in which realistic physiological parameters can be tested *in-silico*, thus presenting an attractive strategy for investigating responses of SW to stimulation, prior to more focused experimental studies.[4] The effects of gastric pacing on a virtual tissue framework have been studied previously.[11] However, earlier studies were limited to a predefined ICC membrane potential trace to represent ICC electrical activity, controlled by an underlying automata algorithm which determined if the surrounding cells were active or at rest. The method was effective for predicting the entrainment induced as a result of an external stimulus, but it lacked a realistic biophysical basis and could not enable predictive physiological studies.

Entrainment has been previously modeled using the biophysically-based Corrias and Buist (CB) ICC model [6] in two different studies.[2,10] In the study of Du et al.[10], an existing voltage-dependent IP3 pathway from Imtiaz et al.[16] was incorporated to enable entrainment. Depolarization of a neighboring ICC evoked changes in the membrane potential, in response to which intracellular Ca^{2+} was released, thereby entraining the slow wave activity of one ICC to other surrounding ICC. In another study by Buist et al.[2], the pacemaker unit was modified with an additional current from voltage dependent dihydropyridine-resistant calcium channels and a Ca^{2+} extrusion current to maintain homeostasis. Adding a voltage-dependent pathway for modulating $[Ca^{2+}]_i$ in the PMU to the original ICC CB model enabled entrainment of the pacemaker mechanism. In both cases, the conduction velocity was primarily dependent on the IP3 parameter which changed the intrinsic pacing frequency and the activation time; and to a lesser degree was dependent on the tissue conductivity parameters. Hence, both studies were unable to incorporate the effects of anisotropic tissue conductivities and propagation patterns in the tissue-level electrophysiology. This is an important limitation, because anisotropic conduction is now known to be a key feature of slow wave conduction, especially during dysrhythmias.[24] Additionally, these models were not able to realistically simulate the effects of external stimuli.

In this study, we present a new method for modelling SW propagation with a biophysically-based reaction term, which was then applied to experimental studies for investigating entrainment, and the effects of gastric pacing on entrainment. The new model has the potential for investigating gastric pacing protocols and the effects of tissue parameters such as anisotropic conductivities along different fiber directions, ICC network-function relationships and the effects of pharmacological agents on SW activity.

2. Materials and Methods

2.1. Entrainment mapping in gastric pacing and gastric transection

Initial parameters to guide the model were based on experimental data from the following experimental studies.

High-resolution experimental recordings of slow wave entrainment during gastric pacing were demonstrated by O'Grady et al. [23] These recordings were obtained using flexible printed-circuit board arrays [9] (8 × 24 electrodes; spacing 7.62 mm; dimensions approx. 6 × 18 cm) placed on a serosa of the anterior gastric corpus of a weaner pig model. Pacing was achieved using bipoloar electrodes implanted into the stomach musculature with the stimulus applied extracellularly in the gastric corpus, and connected to a DS8000 multichannel stimulator (World Precision Instruments, Sarasota, FL).

Hinder et. al. [14] described the acute effects of surgical transection on human gastric electrical activity. The electrical activity was recorded with sparse arrangements of electrodes before and after transection. The electrical activity before transection indicated a consistent frequency potential propagating aborally. However, electrical activity after transection was found to operate at 3 cpm around the corpus region and 1 cpm in the antrum.

2.2. Finite state machine (FSM) approach

Ca^{2+} dynamics play a crucial role in the ICC pacemaking mechanism as inhibition of Ca^{2+} release and SERCA Ca^{2+} uptake has been shown to inhibit SWs in mice and guinea-pigs. [15,28,30] Voltage dependent Ca^{2+} dynamics were developed using a two-state approach where the SW of a gastric cell model, i.e. the ICC CB model, was modeled containing two states: *active* and *passive* (FSM-CB ICC model) as illustrated in Fig. 1.

Our modified cell model was developed using a Mealy finite-state machine approach, where the state of the system depends both on the input conditions and the present state, while diffusion-based propagation actively propagates along the domain. The approach takes advantage of the oscillatory behavior of the ionic and gap junction currents where the start of each *active* state is evaluated with the state variables reinitialized (explained further in section 2.2.3). The state variable values chosen for initialization were based on their values at the time of the start of the excitation phase. In this method, the state transition of the cell model was determined by: a voltage threshold (V_{th}), $[Ca^{2+}]_i$ detector variable (DC), the time for which the cell was in the *passive* period (non-refractory period or NRP) and the start time which changes the cell from initial state to the *active* state (startTime). The state transition diagram is summarised in Fig. 2. The intrinsic frequency is given by (1). Here refractory period (RP) is the *active* period duration which solely depends on the biophysical cell model description and IP3 which is known to regulate the slow wave frequency.[17]

$$f=\frac{1}{(RP+NRP)} \quad (1)$$

2.2.1. $[Ca^{2+}]_i$ tracker—Uptake and release of Ca^{2+} from stores in the endoplasmic reticulum causes a change in $[Ca^{2+}]_i$ and this has been widely accepted as a key signal for the ICC pacemaking mechanism.[18] Additionally, in the ICC-CB model IP3 dependent Ca^{2+} dynamics plays a critical role in controlling the width of the plateau phase. [6] Thus, in the present study, a change in $[Ca^{2+}]_i$ determines the transition from the active to passive state and was prescribed to occur at the point when $\frac{d\left[Ca^{2+}\right]_i}{dt}=0$, indicating a halt in the Ca^{2+} cycling process.

2.2.2. Electrical equivalent of FSM approach—The total current flow through the cell membrane, I_m, is given by

$$I_m=C_m\frac{\mathrm{d}V_m}{dt}+I_{ion} \quad (2)$$

where C_m is the cell membrane capacitance and I_{ion} is the sum of currents $\sum I_{x_n}$ through different ionic channels. The electrical behaviour of the FSM based approach is summarised in Fig. 3., where the output from the FSM controls either the inclusion or exclusion of the cell membrane active components using a switch S1. When the FSM output is *active*, the cell active processes are included representing *active* state or otherwise excludes the active components allowing the cell membrane to behave passively.

2.2.3. Solution process of tissue electrophysiology—A continuum modelling approach is widely used in the gastrointestinal field to quantify tissue electrophysiology.[4] These models are typically semi-implicit in time, where the linear diffusion terms are modeled implicitly and the reaction terms explicitly. Using this approach, V_m is obtained from the solution of PDE and then applied to reaction terms. The reaction terms are solved using an appropriate ODE solver such as the forward-Euler method. In our simulations the solutions were computed using CHASTE modelling software.[21] Following this approach, our solution process was modified as:

1. Diffusion terms were evaluated for the next transmembrane potential V_m with the evaluated transmembrane ionic current I_{ion}. The next state of the cell model was identified based on the state transition diagram as shown in Fig. 2. If the next state was *passive*, then step 2 was evaluated; or if the next state was *active*, then step 3 was evaluated.
2. The ionic processes were made virtually inactive while passively conducting the diffused potential V_m. This was implemented by:

$$\frac{ds}{dt}=0 \quad (3)$$

$$I_{ion}=0 \quad (4)$$

   where *s* denotes the state variables.
3. If there was a transition from *passive* to *active* state, the Ca^{2+} dynamics was initiated by evaluating the derivatives with initial conditions; otherwise, continue evaluating from the previously evaluated derivative values using:

$$\frac{ds}{dt}=f\left(s, V_m, t\right) \quad (5)$$

$$I_{ion}=F\left(s, V_m\right) \quad 6$$

   where *f* and *F* are determined by the cell model.
4. If there was a transition from *active* to *passive* state, then the state variables were reinitialized to their initial values to represent the start of activation of the Ca^{2+} dynamics.
5. Go to step 1.

2.3. Tissue model setup

2.3.1. Stomach transection study model—In our tissue model setup, a monodomain model was used with surface area to volume ratio, χ = 2,000 cm $^{-1}$; membrane capacitance, C_m = 2.5 μF cm $^{-2}$; conductivity, σ = 0.04 mS cm^{-1} and V_{th} = −55 mV. These parameters were chosen to closely match gastric SW propagation velocities observed in human corpus, i.e., ~3 mm s^{-1}. The geometry was a 128 mm long 1-D model comprised of finite elements with node resolution of 1 mm. Based on the stomach transection study of Hinder et al.[14], a linear gradient of intrinsic frequency ranging from 3 cpm to 1 cpm was set using the parameter NRP. Two models representing normal and uncoupled stomach activity were simulated, with all cells corresponding to FSM-CB ICC model. In the normal simulation, all the cells were electrically coupled together, while in the uncoupled simulation the stomach

was divided into three equal segments by reducing the conductivity values between the segments to 0.01 nS cm^{-1}.

2.3.2. Gastric pacing induced entrainment mapping study model—Initially, we studied the effect of external pacing on entrainment using the 1-D model (Section 2.3.1). SWs were simulated until steady state was attained. Following steady state, a periodic stimulus pulse of 5 ms duration and amplitude 12000 μA cm^{-3} was applied at frequency 3.75 pulses per minute to the bottom node to analyse its effect on native SW activity. The tissue was paced using the point stimulus option available in CHASTE, i.e. extracellularly with a return electrode in the intracellular space.[25]

We extended our simulations to a two-dimension high-resolution mapping framework previously applied in porcine gastric pacing trials (section 2.1.2).[23] In our simulation setup, the stomach region covered by the electrode array (see Section 2.1.2) was represented using a finite element triangular mesh with a total of 11,041 nodes and, additionally surrounded by a virtual volume conducting bath of thickness 1 cm to extend the extracellular space and realistically represent the experimental set-up. The average inter-nodal spacing was 1 mm. The novel FSM-CB ICC model was again used as a description of the cell activity at each solution point. Based on the experimental recording, a bidomain model was developed with parameters chosen to represent the experimental recordings of normal antegrade slow wave propagation. The surface area to volume ratio, χ =2,000 cm^{-1} ; membrane capacitance, C_m = 2.5 μF cm^{-2}; intracellular conductivities parallel and perpendicular to fiber as σ_{ix} = 0.175 mS cm^{-1} and σ_{iy} = 0.0665 mS cm^{-1} ; extracellular conductivities parallel and perpendicular to fiber as σ_{ex} =0.7 mS cm^{-1} and σ_{ey} = 0.84 mS cm^{-1} and threshold voltage of excitation of cell, V_{th} = −55 mV. The tissue fibres were oriented parallel to the x-axis. The diffusion terms were solved with a time step of 0.1 ms and reaction terms were solved using the forward-Euler method, also with a time step of 0.1 ms. Native SW activity with an intrinsic frequency 3.16 cpm was initiated at the top left corner of the virtual tissue field by allowing that cell to activate at t = 0 s. A periodic stimulus current was then introduced into the mid-portion of the simulation setup, in analogous manner to the experimental framework, with amplitude 12,000 μA cm^{-3} and a period of 17 s (3.53 pulses per minute). This chosen stimulus raised the transmembrane potential to V_{th} = −55 mV.

3. Results

3.1. Comparison of FSM-CB ICC model vs. original ICC CB model

A monodomain model with tissue parameters as detailed in Section 2.3.1 was used for analysing the implications of FSM based approach on the stablity of ICC response. The response of a single cell of the newly developed FSM-CB ICC model was compared to that of the original ICC model by performing two simulations; the first having all nodes corresponding to the original ICC CB model, and the second having the membrane responses corresponding to the novel FSM-CB ICC model. Diffusion terms were solved with a time step of 0.1 ms and the reaction component was solved using a forward-Euler method, also with a time step of 0.1 ms.

The sum of ionic currents (for a single node) for both FSM-CB ICC model and default CB ICC model is shown in Fig. 4A. In the corresponding V_m trace (Fig. 4C), there was a ~1 mV (< 2% of net depolarization amplitude) downstroke before the onset of primary component amplitude. Furthermore, the V_m trace showed a sharp peak in the primary component amplitude. Additionally, the change in the ionic current trace for ICC CB model was gradual, whereas it was rapid in the FSM based approach (compare Fig. 4A and Fig. 4B). However, the morphology of the waveform with the two important components, i.e, primary component amplitude and a plateau phase, were retained.

During the *passive* state, the external stimulus current was able to drive the FSM based cell to *active* state. In contrast, during the *active* state the external current did not have any effects on the cell activity as shown in Fig. 4C. Likewise, an external stimulus had no significant effect on ICC CB model Fig. 4D.

Finally, a simulation was performed for 420 s to analyse the stability of the FSM-CB ICC model. A train of stimulus currents (amplitude 12,000 $\mu A\ cm^{-3}$; pulse width 5 ms; frequency 4 cpm for total duration of 170 s) was applied at 140 s (Fig. 4E). Simulation results showed that the ICC initially excited at its intrinsic frequency of 3 cpm until 140 s, after which the ICC excited at 4 cpm for 165 s. After stimulation ceased, activity returned back to its intrinsic frequency of 3 cpm (Fig. 4E).

3.2. Analysis based on experimental observations

3.2.1. Effect of uncoupled block of tissue on entrainment—Traces were sampled from cells at 8 mm intervals along the 128 mm geometry for both normal and uncoupled model as shown in Fig. 5. The normal simulation resulted in all the cells being entrained to the highest intrinsic frequency of 3 cpm. In the uncoupled simulation each virtually isolated segment was entrained to the highest intrinsic frequency in that particular segment. The isolated entrained frequencies were 3, 2.4 and 1.7 cpm respectively.

3.2.2. Effects of gastric pacing on normal slow wave propagation—Traces were sampled from cells at 8 mm intervals along the 128 mm line of tissue. Simulations were run until steady-state where all cells were entrained to 3 cpm, corresponding to the highest intrinsic frequency. External pacing resulted in a progressive entrainment of SWs over the entire field at 3.75 cpm (equivalent to the pacing frequency) as seen in Fig. 6.

The experimental and the corresponding simulated activation maps for the 2D normal antegrade activation, gradual entrainment of the mapped field over successive cycles of pacing, and complete entrainment are shown in Fig. 7. The simulated slow wave activity was in agreement with the experimental recordings in terms of the velocities, propagation pattern and entrainment pattern. In both virtual and experimental cases, slow waves propagated antegrade with matching conduction velocities. The propagation velocity in the circular direction was ~9 $mm\ s^{-1}$; compared to ~5 $mm\ s^{-1}$ longitudinally which was comparable with experimental observations. Slow wave activation maps were generated as shown in Fig. 7B. The entire field was entrained in 180 s after the onset of stimulus pacing. The pacing entrainment gain was uniform in the retrograde direction while clashing against the natural antegrade slow waves as shown in Fig. 7B.

3.3. Computational performance

The efficiency gain in the computational performance of the FSM based approach was significant as the solution process during the *passive* state does not require solving the system of ODEs. We used a monodomain model with 51 solution points corresponding to either FSM-CB ICC model or the original ICC CB model. Since the computational time depends on the number of *active* phases and *passive* phases, all the nodes were implemented to excite at the same time so as to have equal number of *passive* and *active* phases.

The relative computational performance was found to not only depend on the type of cell model but also at which frequency the simulation was performed. The average computational time required for solving the ODEs for 120 s of simulation time with the ICC intrinsic frequency of 3 cpm was recorded using the internal CHASTE profiler. These were obtained as 75.0 ± 1.1 s (n=5) and 119.4±1.3 s (n=5) for FSM-CB ICC and ICC CB respectively on an Intel® Core TM i5 processor 2410M machine, which implied the default

CB ICC model was 59% more expensive compared to the novel FSM-CB ICC model. Further, computational performance for simulations with a low intrinsic frequency of 2 cpm were also compared. The performance for ICC CB model with intrinsic frequency of 2 cpm was comparable with that of intrinsic frequency of 3 cpm which was found to be 120.5 ±1.1 s (n=5). However, this time the computational performance for FSM-CB ICC model was 51.4 ± 0.3 s (n=5), implying the ICC CB model was 134% more expensive compared to FSM-CB ICC model.

4. Discussion

This study presents a new computational method for analysing gastric SW entrainment and the effects of gastric pacing on SW activity by applying a biophysically-based ICC CB cell. This method successfully simulated the effects of external stimuli, entrainment by a higher frequency external pacing stimulus and finally captured the effects of anisotropic conduction on SW propagation, showing good agreement with experimental recordings. The model was tested for baseline drift over time, and was assessed for its behaviour before/after a series of external stimuli. The model was stable and returned to its natural intrinsic frequency once pacing was suspended. Furthermore, there was no significant effect on the underlying mechanics of cellular electrical behaviour in the native cell model with the FSM modification, and major gains in computational efficiency were evident.

Three significant advances in GI mathematical modeling have been achieved in establishing this modelling framework. Firstly, an ICC entrainment model, where the SW propagation depends on the electrical parameters of tissue (fiber direction and conductivities), was successfully developed with a biophysically based cell model. The ICC CB model was chosen for this study as it was successfully applied to reproduce the ICC ionic mechanisms and responds predictively to real physiological parameters such as voltage and electrolyte concentrations. Until now, GI simulations had conduction velocity and slow wave propagation dynamics in part determined by the underlying intrinsic frequency distribution. Now, realistic biophysically based multiscale simulations over complex gastric tissue structures can be achieved. Secondly, this study was the first to accurately model the effects of gastric pacing on entrainment using a biophysically based cell model. Effects of gastric pacing were validated against high-resolution mapping experimental data. This model will enable the effects of pacing to be predicted with consideration of anistropic tissue properties, which are critical for the initiation and maintenance of dysrhythmic patterns, particularly in humans.[22,24] Finally, the computational performance analysis indicated an efficient solution process with the bottleneck limited to the spatial solution points in the *active* duration. The time spent during the *active* state was the same as that of the original ICC CB model for each time step without using the FSM based approach. Furthermore, the methods were successfully applied to the monodomain and bidomain frameworks and can be readily extended to the extended-bidomain framework.[3]

The ICC pacemaking mechanism is thought to be dependent on Ca^{2+} entry through a voltage dependent mechanism.[28] The method presented here modulates the Ca^{2+} dynamics by activating them in the *active* state and disabling them while transiting to the *passive* state. The pacemaking mechanism and its biophysical dependence do not change with this modification. The *active* phase of the gastric cell model solely depends on its native ionic mechanisms. Any gastric cell model with a biophysical *active* response can be included as a reaction term in this model framework. The method promises a new direction where researchers can now concentrate on the ionic mechanisms involved in the refractory phase of gastric ICC cell activity. Accordingly, the effects of ion channel pathologies can also be implemented into this framework as their details are revealed, and pharmaceutical agents for

targeting normal and abnormal channel properties can also be evaluated in-silico prior to experimental applications.[26]

The impact of the FSM approach on the CB model were detailed in Section 3.1. This showed a small change in the potential morphology when compared with the original CB model. There was a downstroke of ~1 mV before the depolarization stroke, and a more distinguishable primary amplitude compared to the plateau phase. It should be noted that, at the macroscopic scale relevant to the application of this model and while considering the variability in the morphology of slow wave recordings, the simulated slow wave was consistent with experimental observations,[15] and remains dependent on the biophysical basis of the underlying cell model. This would be largely avoided if the refractory phase alone of cell behaviour was modeled while ignoring the non-refractory period. Furthermore, this would potentially also elicit a significant performance improvement. A detailed analysis of the individual ionic currents indicated that reinitializing the state variable affects most of the ionic channels in the FSM-CB ICC model. The Na^+ ion current (I_{Na}) analysis showed an increased rate of influx of ions (0 to ~12 pA cm^{-3}) flowing through the Na^+ channels when compared with ICC-CB model (~6 to ~10 pA cm^{-3}) and can be reasoned from the observation that in the ICC-CB model, there was an active sodium current (~6 pA cm^{-3}) during the non-refractory phase, whereas in our FSM-CB ICC model the I_{Na} current was inactive (0 A) during that period, which agrees better with experimental studies (Refer Appendix).[1] The sharp distinguishable primary component and the plateau phase can then be attributed to a increased rate of change of I_{Na} current when the state changes from *passive* state to *active*.

The effects of external pacing on slow wave activity were simulated on an ICC network, whereas the experimental recordings were obtained from tissue containing both ICC and smooth muscle cells (SMC). The effect of this coupling has been evaluated by simultaneous intracellular recordings of slow wave activity in SMC and ICC which showed that slow waves originate in ICC and conduct to SMC.[8] However, the coupling between ICC and SMC occurs without draining excessive current, such that ongoing entrainment in the ICC networks would be affected.[7]

This model can be used to develop new therapeutic approaches for motility disorders and obesity. In obesity, gastric pacing has been used to disrupt normal antegrade slow-wave activity by inducing retrograde events, thereby slowing motility and inducing satiety.[29] However, current progress has been limited by the need to increase efficiency in pacing protocols and optimize pacing sites. The cell model presented here provides an ideal platform for rapidly achieving such investigations without the need for exhaustive animal trials.

It should be noted that there is limited experimental data to inform the choice of simulation parameters. For example, an outstanding question is: what is the stimulus current or voltage required to just excite and initiate the pacemaking mechanism? In this study, the tissue electrical parameters were chosen to replicate the conduction velocity observed in experimental studies.[23] A limitation in this model is uncertainty over the effects of current inputs from the neighbouring cells on the ionic channels during the passive period. The model incorporates the effects of external current by accumulating the charge across the cell membrane while increasing the V_m until V_{th}. However, it remains an open biophysical question as to the ion channels being affected by the external currents.

In conclusion, we have presented a model framework that provides a major advance over previously published models. This framework, with further incorporation of anatomical and

smooth muscle model physiology,[5] will potentially be an important tool for analysing gastric electrophysiology in normal and diseased states.

Acknowledgments

This work was supported in part by grants from the Riddet Institute, New Zealand, Health Research Council, New Zealand and NIH (R01 DK 64775). The authors thank Mr. Niranchan Paskaranandavadivel at the Auckland Bioengineering Institute for his suggestions.

Appendix A

Table 1. Values used for reinitializing the state variable.

Table 1

State variable initialization values

State Variables	Value
Ca_i	1.00313877561076e-5
d_{Ltype}	8.2129376673855e-6
f_{Ltype}	0.940875545921428
f_ca_Ltype	0.999999999916296
d_{VDDR}	0.000980476616434842
f_{VDDR}	0.567152727511813
d_{CaCl}	0.000367480059580162
d_{ERG}	0.200000000002862
d_{kv11}	0.00398797223045225
f_{kv11}	0.997147049083731
d_{Na}	0.0137236312559018
f_{Na}	0.181419340228229
d_{NSCC}	0.00504356407198514
PU_unit-Ca_{PU}	7.540777440001e-5
PU_unit-Ca_m	0.000230865523129487
PU_unit-Ca_{ER}	0.00322893516976944
PU_unit-ADP_m	2.60102039587125
PU_unit-ADP_i	0.00772882663640341
PU_unit-$NADH_m$	0.101697199557924
PU_unit-h	0.939672799158766
PU_unit-deltaPsi	163.99886497951

Appendix B

The following plots show the comparison of different ionic channel currents describing the ICC cell behaviour for FSM-CB model and ICC-CB model.

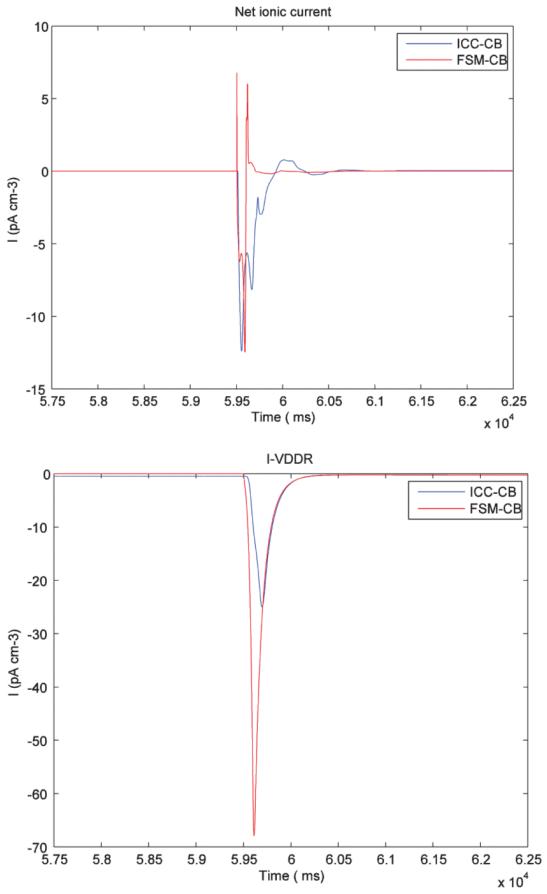

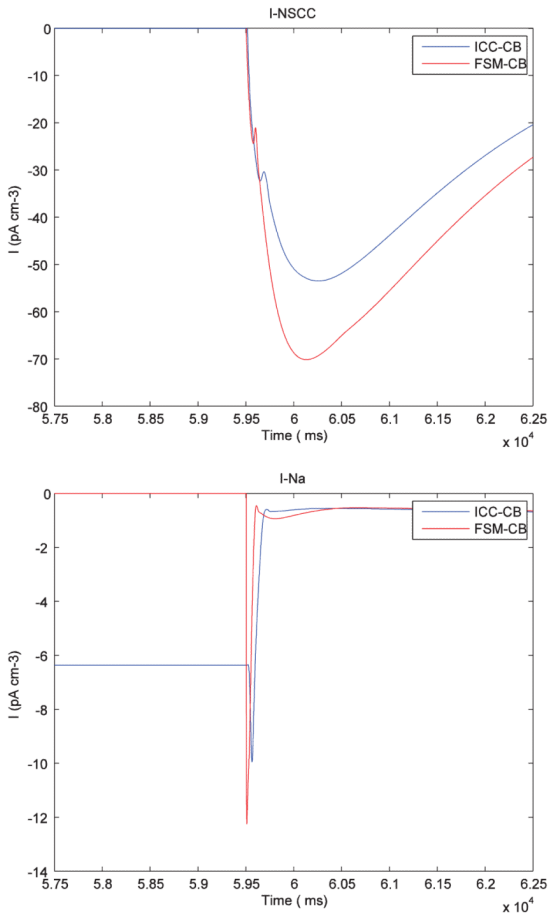

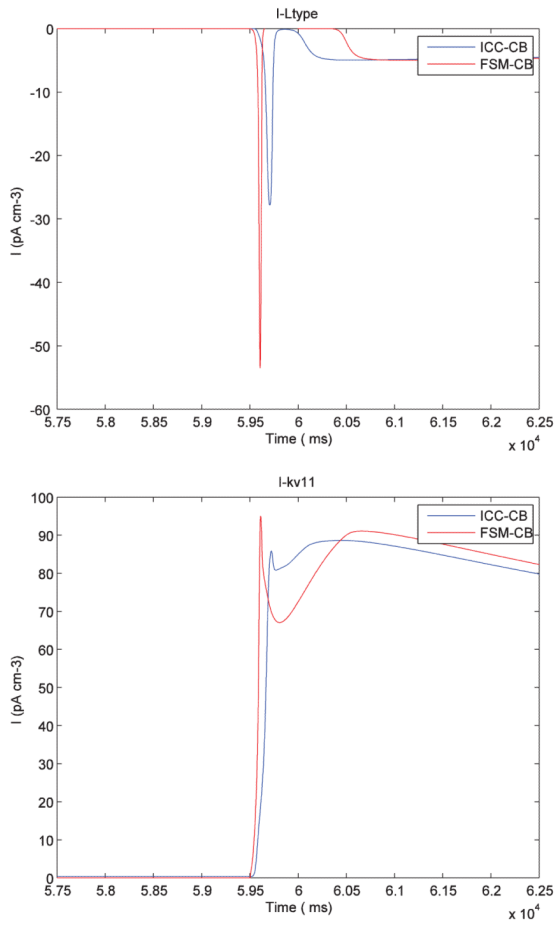

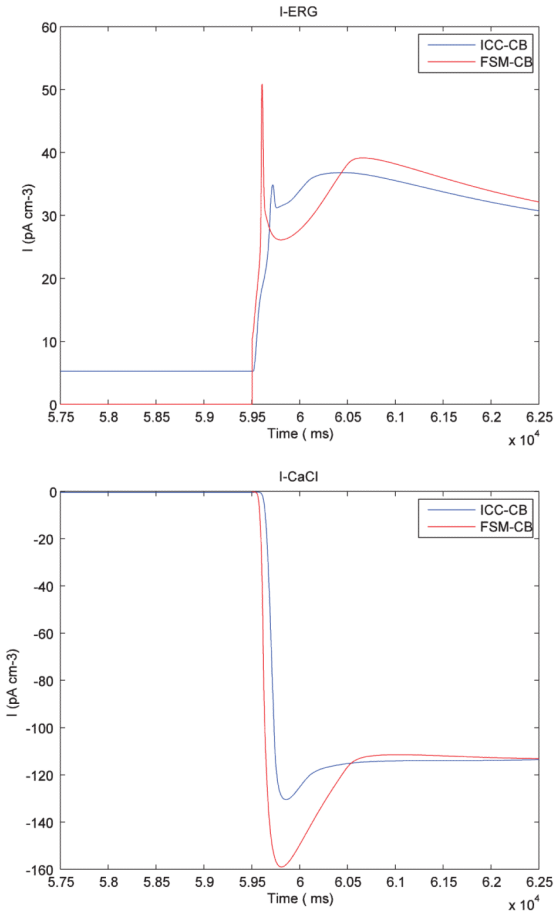

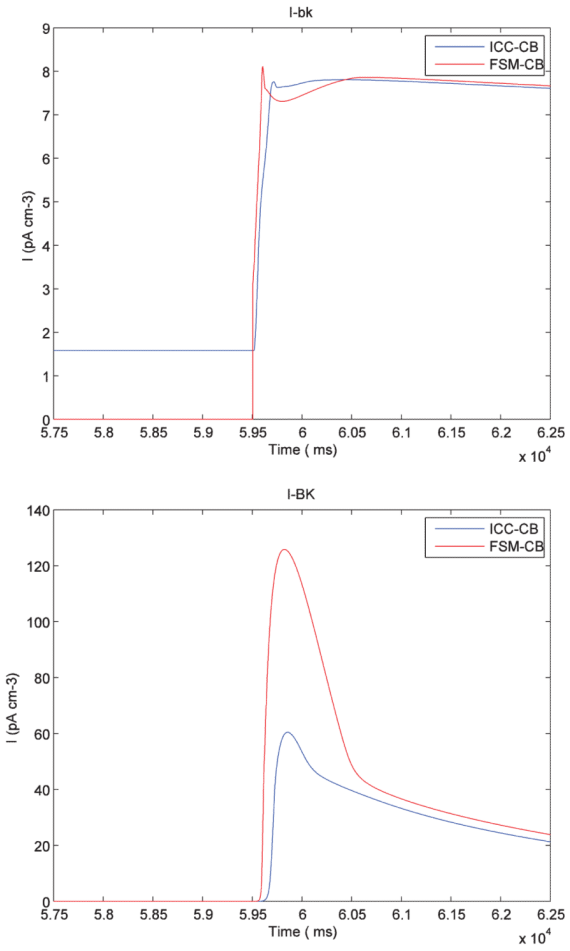

References

1. Beyder A, Rae JL, Bernard C, Strege PR, Sachs F, Farrugia G. Mechanosensitivity of Nav1.5, a voltage-sensitive sodium channel. J. Physiol. 2010; 588:4969–85. [PubMed: 21041530]
2. Buist ML, Corrias A, Poh YC. A model of slow wave propagation and entrainment along the stomach. Ann Biomed Eng. 2010; 38:3022–30. [PubMed: 20437204]
3. Buist ML, Poh YC. An extended bidomain framework incorporating multiple cell types. Biophys. J. 2010; 99:13–8. [PubMed: 20655828]
4. Cheng LK, O'Grady G, Du P, Egbuji JU, Windsor JA, Pullan AJ. Gastrointestinal system. Wiley Interdiscip Rev Syst Biol Med. 2010; 2:65–79. [PubMed: 20836011]
5. Corrias A, Buist ML. A quantitative model of gastric smooth muscle cellular activation. Ann Biomed Eng. 2007; 35:1595–607. [PubMed: 17486452]
6. Corrias A, Buist ML. Quantitative cellular description of gastric slow wave activity. Am J Physiol Gastrointest Liver Physiol. 2008; 294:G989–95. [PubMed: 18276830]
7. Cousins HM, Edwards FR, Hickey H, Hill CE, Hirst GDS. Electrical coupling between the myenteric interstitial cells of Cajal and adjacent muscle layers in the guinea-pig gastric antrum. J. Physiol. 2003; 550:829–44. [PubMed: 12844505]
8. Dickens EJ, Hirst GD, Tomita T. Identification of rhythmically active cells in guinea-pig stomach. J. Physiol. 1999; 514(Pt 2):515–31. [PubMed: 9852332]
9. Du P, O'Grady G, Egbuji JU, Lammers WJ, Budgett D, Nielsen P, Windsor J. a, Pullan a J. Cheng LK. High-resolution mapping of in vivo gastrointestinal slow wave activity using flexible printed

circuit board electrodes: methodology and validation. Ann Biomed Eng. 2009; 37:839–46. [PubMed: 19224368]

10. Du P, O'Grady G, Gibbons SJ, Yassi R, Lees-Green R, Farrugia G, Cheng LK, Pullan AJ. Tissue-specific mathematical models of slow wave entrainment in wild-type and 5-HT(2B) knockout mice with altered interstitial cells of Cajal networks. Biophys. J. 2010; 98:1772–1781. [PubMed: 20441740]
11. Du P, O'Grady G, Windsor JA, Cheng LK, Pullan AJ. A tissue framework for simulating the effects of gastric electrical stimulation and in vivo validation. IEEE Trans. Biomed. Eng. 2009; 56:2755–61. [PubMed: 19643697]
12. El-Sharkawy TY, Morgan KG, Szurszewski JH. Intracellular electrical activity of canine and human gastric smooth muscle. J. Physiol. 1978:291–307. [PubMed: 671352]
13. Farrugia G. Interstitial cells of Cajal in health and disease. Neurogastroenterol Motil. 2008; 20(Suppl 1):54–63. [PubMed: 18402642]
14. Hinder RA, Kelly KA. Human gastric pacesetter potential. Am. J. Surg. 1977; 133:29–33. [PubMed: 835775]
15. Hirst GD, Edwards FR. Generation of slow waves in the antral region of guinea-pig stomach--a stochastic process. J. Physiol. 2001; 535:165–80. [PubMed: 11507167]
16. Imtiaz MS, Smith DW, van Helden DF. A theoretical model of slow wave regulation using voltage-dependent synthesis of inositol 1,4,5-trisphosphate. Biophys. J. 2002; 83:1877–90. [PubMed: 12324409]
17. Kim TW, Koh SD, Ordog T, Ward SM, Sanders KM. Muscarinic regulation of pacemaker frequency in murine gastric interstitial cells of Cajal. J. Physiol. 2003; 546:415–425. [PubMed: 12527728]
18. Lees-Green R, Du P, O'Grady G, Beyder A, Farrugia G, Pullan AJ. Biophysically based modeling of the interstitial cells of Cajal: current status and future perspectives. Front Physiol. 2011; 2:29. [PubMed: 21772822]
19. Lin ZY, McCallum RW, Schirmer BD, Chen JDZ. Effects of pacing parameters on entrainment of gastric slow waves in patients with gastroparesis. Am J Physiol Gastrointest Liver Physiol. 1998; 274:G186–G191.
20. McCallum RW, Chen JD, Lin Z, Schirmer BD, Williams RD, R. R. Gastric pacing improves emptying and symptoms in patients with gastroparesis. Gastroenterology. 1998; 114:456–61. [PubMed: 9496935]
21. Mirams GR, Arthurs CJ, Bernabeu MO, Bordas R, Cooper J, Corrias A, Davit Y, Dunn S-J, Fletcher AG, Harvey DG, Marsh ME, Osborne JM, Pathmanathan P, Pitt-Francis J, Southern J, Zemzemi N, Gavaghan DJ. Chaste: An open source C++ library for computational physiology and biology. PLoS Comput. Biol. 2013; 9:e1002970. [PubMed: 23516352]
22. O'Grady G, Angeli TR, Du P, Lahr C, Lammers WJEP, Windsor J. a, Abell TL, Farrugia G, Pullan AJ, Cheng LK. Abnormal initiation and conduction of slow-wave activity in gastroparesis, defined by high-resolution electrical mapping. Gastroenterology. 2012; 143:589–98.e1–3. [PubMed: 22643349]
23. O'Grady G, Du P, Lammers WJEP, Egbuji JU, Mithraratne P, Chen JDZ, Cheng LK, Windsor JA, Pullan AJ. High-resolution entrainment mapping of gastric pacing: a new analytical tool. Am J Physiol Gastrointest Liver Physiol. 2010; 298:G314–21. [PubMed: 19926815]
24. O'Grady G, Du P, Paskaranandavadivel N, Angeli TR, Lammers WJ, Asirvatham SJ, Windsor JA, Farrugia G, Pullan AJ, Cheng LK. Rapid high-amplitude circumferential slow wave propagation during normal gastric pacemaking and dysrhythmias. Neurogastroenterol Motil. Jul; 2012 24(7):e299–312. [PubMed: 22709238]
25. Pathmanathan P, Bernabeu MO, Bordas R, Cooper J, Garny A, Pitt-Francis JM, Whiteley JP, Gavaghan DJ. A numerical guide to the solution of the bi-domain equations of cardiac electrophysiology. Prog. Biophys. Mol. Bio. 2010; 102:136–55. [PubMed: 20553747]
26. Poh YC, Beyder A, Strege PR, Farrugia G, Buist ML. Quantification of gastrointestinal sodium channelopathy. J Theor Biol. 2012; 293:41–8. [PubMed: 21959314]
27. Sanders KM, Koh SD, Ward SM. Interstitial cells of Cajal as pacemakers in the gastrointestinal tract. Annu. Rev. Physiol. 2006; 68:307–343. [PubMed: 16460275]

28. Ward SM, Dixon RE, de Faoite A, Sanders KM. Voltage-dependent calcium entry underlies propagation of slow waves in canine gastric antrum. J. Physiol. 2004; 561:793–810. [PubMed: 15498805]

29. Yin J, Chen JDZ. Implantable gastric electrical stimulation: ready for prime time? Gastroenterology. 2008; 134:665–7. [PubMed: 18325383]

30. Suzuki H, Hirst GD. Regenerative potentials evoked in circular smooth muscle of the antral region of guinea-pig stomach. J Physiol. Jun 1; 1999 517(Pt 2):563–73. [PubMed: 10332102]

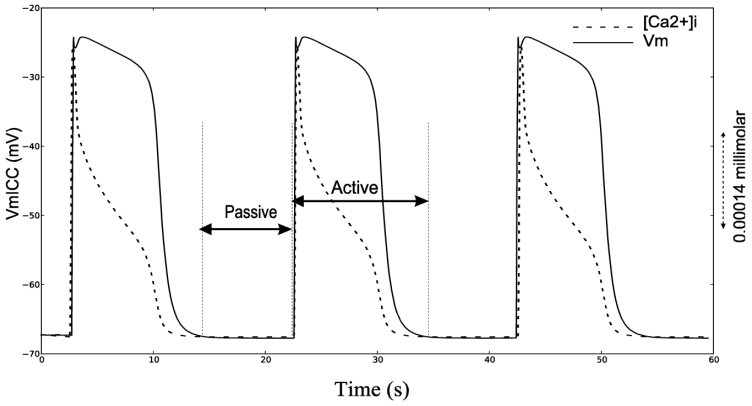

Fig. 1.
Simulated gastric ICC cell activity (solid line) and trace of corresponding $[Ca^{2+}]_i$ (dashed line) using ICC-CB model.

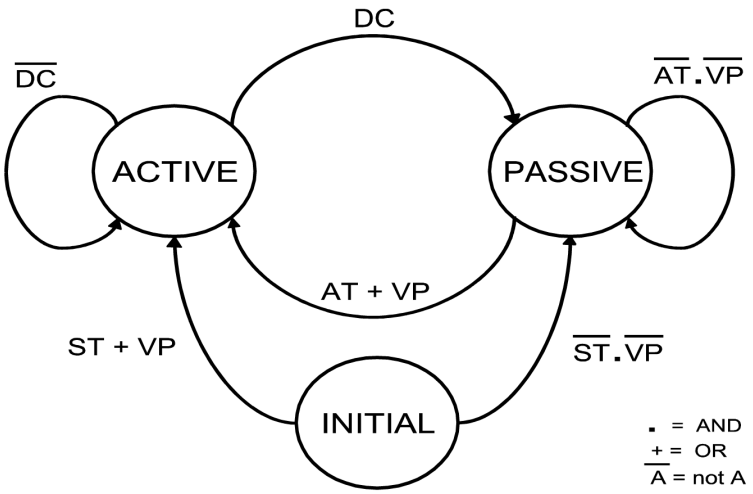

Fig .2.

State transition diagram for the finite state machine equivalent of ICC model. ST indicates if time has passed the *startTime*, which is set as a parameter and which determines initial excitation when there is no threshold voltage coming into the model. AT indicates if the NRP has been passed and signals transition from *passive* state to *active* state. The variable NRP determines the intrinsic frequency of the ICC cells along with IP3 parameter. DC identifies if the change in concentration of intracellular Ca^{2+} has returned to quiescent state. VP variable is set to true if there is a voltage which is greater than the V_{th} of the cell.

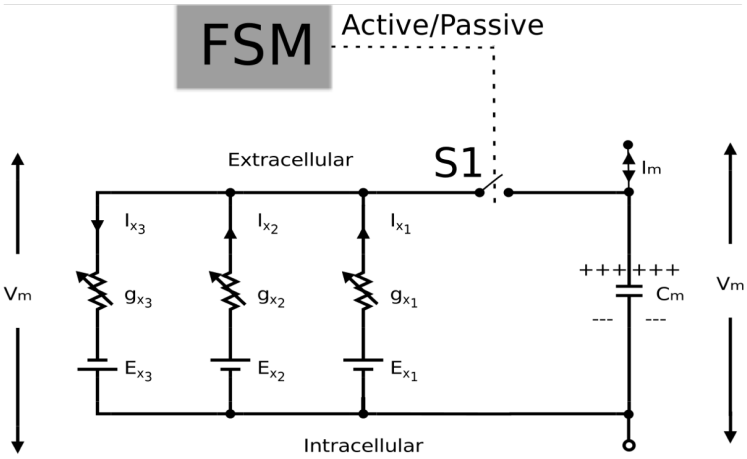

Fig. 3.

Electrical circuit equivalent for FSM based gastric cell behaviour that represents the current across the cell membrane. The switch S1 is controlled by the FSM which is turned on or off depending on whether the output of FSM is *active* or *passive* respectively.

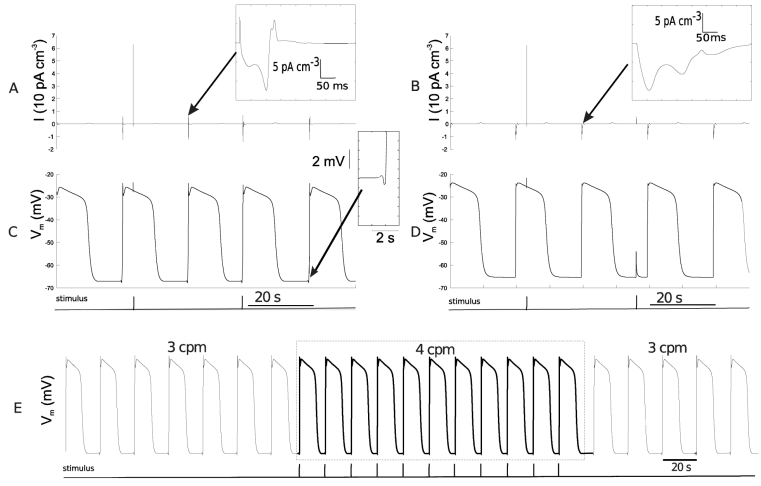

Fig. 4.

Comparison of the FSM-CB ICC with the ICC CB model. (A) Plot of the summation of all ionic currents and (C) transmembrane potential plot for the FSM-CB ICC model, and in (B) and (D) the corresponding plots for ICC CB model. (E) V_m trace for a single FSM-CB ICC which was stimulated at the rate of 4 cpm for duration of 165 s for a total duration of 410 s with an intrinsic frequency of 3 cpm.

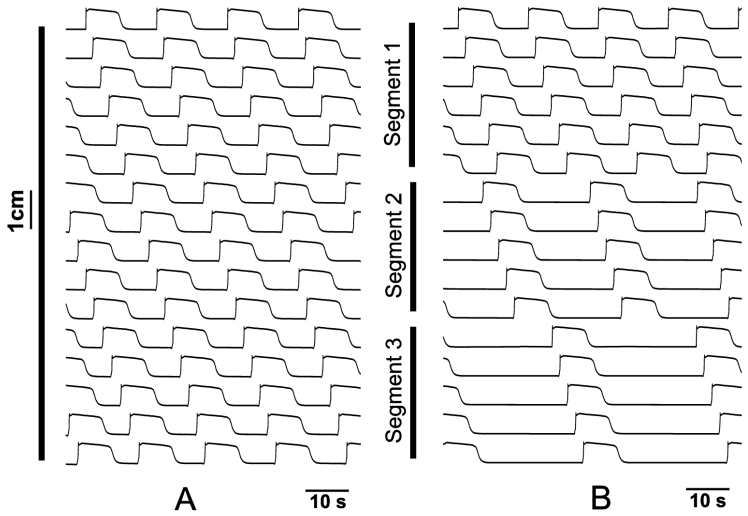

Fig. 5.

Effect of decoupling on entrainment. (A) Spatiotemporal (V_m) trace for simulated slow wave activity on 128 mm long 1-D model sampled at 8 mm intervals for a duration of 80 s. The intrinsic frequency of the ICC was varied linearly from 3 cpm to 1 cpm. All ICC are entrained to the frequency corresponding to the highest frequency of 3 cpm. (B) Spatiotemporal V_m trace when the 1-D model was decoupled into 3 segments by reducing the conductivities between sections to 0.01 nS cm^{-1}. Each uncoupled segment was entrained to the highest intrinsic frequency ICC within that segment.

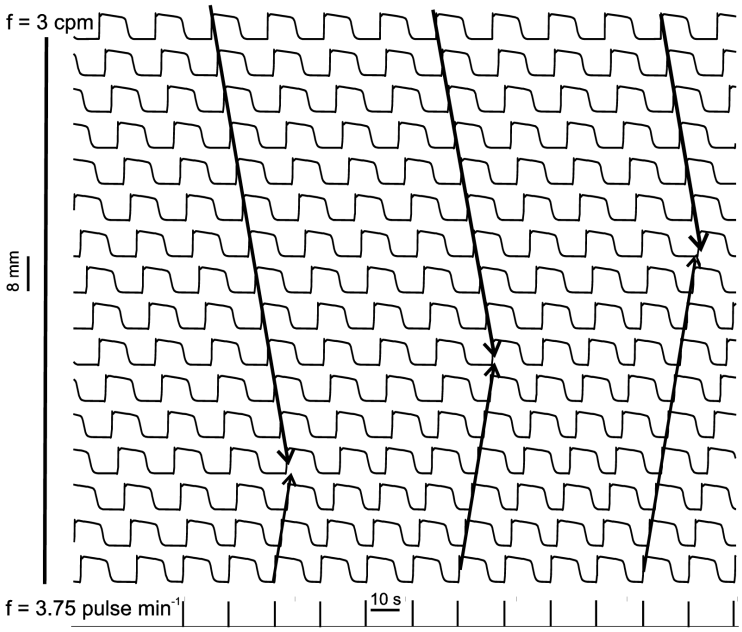

Fig. 6.

Spatiotemporal (V_m) trace for simulated slow wave activity on 128 mm long 1-D model with the recording at 8 mm intervals for a duration of 230 s. The arrows indicate the gradual takeover by the stimulated pulses.

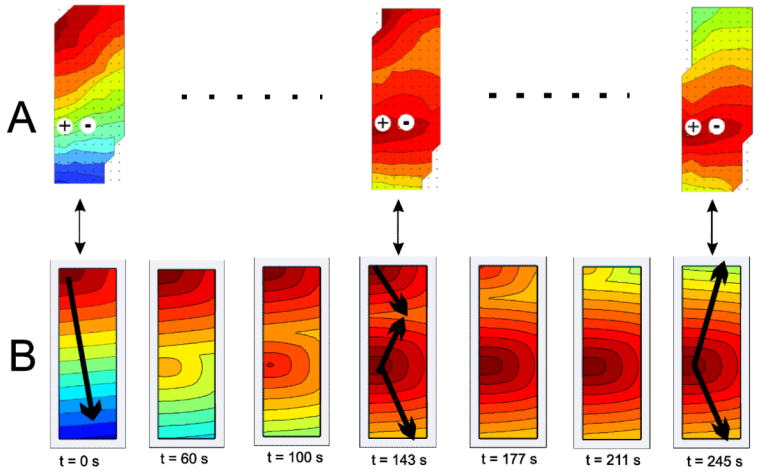

Fig. 7.

Activation maps comparing the experimental and simulated propagation patterns. (A) Activation maps of experimental high resolution mapping, with an isochronal interval of 2 s per color band. An external pacing stimulus was applied to the middle of the mapped field (as denoted by the +/− symbols) to study propagation dynamics, which is shown to progressively entrain or control the entire mapped field. (B) Activation maps showing gradual retrograde entrainment for simulated gastric pacing induced entrainment, with an isochronal interval of 2 s. The tissue model was surrounded by a 10 mm thick virtual bath.